Compressive sampling photoacoustic tomography based on edge expander codes and TV regularization

Zhenghua Wu (伍政华), Mingjian Sun (孙明健)*, Qiang Wang (王 强), Naizhang Feng (冯乃章), and Yi Shen (沈 毅)

Department of Control Science and Engineering, Harbin Institute of Technology, Harbin 150001, China

**Corresponding author: sunmingjian@hit.edu.cn*

Received May 3, 2014; accepted July 3, 2014; posted online September 25, 2014

A new photoacoustic (PA) signal sampling and image reconstruction method, called compressive sampling PA tomography (CSPAT), is recently proposed to make low sampling rate and high-resolution PA tomography possible. A key problem within the CSPAT framework is the design of optic masks. We propose to use edge expander codes-based masks instead of the conventional random distribution masks, and efficient total variation (TV) regularization-based model to formulate the associated problem. The edge expander codes-based masks, corresponding to non-uniform sampling schemes, are validated by both theoretical analysis and results from computer simulations. The proposed method is expected to enhance the capability of CSPAT for reducing the number of measurements and fast data acquisition.

OCIS codes: 100.3020, 110.5120, 170.5120.
doi: 10.3788/COL201412.101102.

Photoacoustic (PA) imaging has emerged as a powerful tool for various biomedical studies, such as molecular imaging of biomarkers, functional imaging of physiological parameters, and gene expression products[1–3]. PA tomography (PAT) is based on the PA effect which refers to the generation of acoustic waves by the absorption of electromagnetic energy, such as optical, radio-frequency, or microwave energy[4–8]. In biomedical applications, laser pulses are delivered into biological tissue. Some of delivered energy will be absorbed and converted into heat, leading to transient thermoelastic expansion and thus wideband acoustic wave emission. The generated acoustic waves are then detected by ultrasound transducer to reconstruct images. PAT has ultrasonic resolution with high tissue contrast due to optical absorption. In addition, compared with other optical imaging, PAT has deeper penetration depth, and provides high resolution at relatively large imaging depth.

For the conventional scanning PAT system, more number of measurements are required to obtain high-resolution images, which imply long data acquisition time and high-cost system. Significant efforts have been made to address this problem, one key approach is to explore the sparsity of PA images and reconstruct the images from limited view acquisitions[9–13]. Recently, a new data acquisition method, compressive sampling PAT (CSPAT), is proposed to make low sampling rate and high-resolution PAT possible by leveraging optic masks[10,14–16]. As shown in Fig. 1, several mirrors deflect

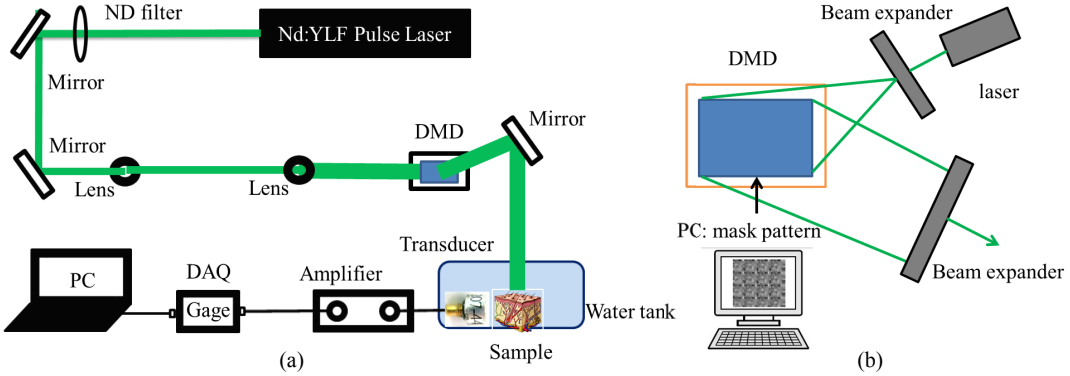

Fig. 1. (a) Schematic representation of CSPAT framework: in practice, the excitation laser can be a diode-pumped Nd:YLF Q-switched pulsed laser (523 nm wavelength, 6 ns pulse width; IS8II-E, INNOSLAB Edgewave, Germany), the maximum pulse repetition rate of the Nd: YLF laser is up to 5 kHz and (b) the principle diagram of DMD (parameters in practice can be: HS200G, 800 × 600 pixel, 0.55 inches for panel size, 0.442.41 inches for projection distance).

the laser beam, adjusting both the direction and elevation. A beam expander then shrinks the laser beam by a 4f optical system, in order to fit the digital mirror device (DMD). The 4f optical system consists of two plano-convex lenses, respectively. A neutral density filter is placed in the middle to smoothen the laser beam profile. The laser beam is then directed onto the DMD for 2D laser scanning of biological tissue. The mask patterns (0-1 matrices) of DMD can be fixed by LabVIEW software on PC. Again, the unfocused transducer receives PA waves at near field, and the signals then go through pre-amp and are recorded by gage data acquisition card. Finally, reconstructed PA images can be obtained to study the biological tissue.

An important issue within the CSPAT framework is how to design the optic masks. The widely used optic masks in the original CSPAT framework are random masks, which are corresponding to the conventional compressive sampling schemes[17]. However, the structures of the significant coefficients in the sparse signals are ignored by data acquisition under the random sampling cases. A representative sparsity structure for a sparse signal can be expressed as sparse sum of subspace (also known as block sparse)[18], which implies the nonzero values always appear in some specific low-dimensional subspaces. In addition, natural signals always have sparse representations in some frequency domain, and the significant coefficients mostly appear at lower frequency. In practical application, sparsity structures are always obtained via dictionary learning or some prior knowledge[18]. Intuitively, the more significant elements of the sparse signals should be captured by more measurements for exact reconstruction. It has been proved that this novel scheme has superior performance than ordinary random sampling schemes[19]. Here we propose to use this novel theory for CSPAT mask design by leveraging edge expander codes[20]. Specifically, we want to reduce the number of measurements by giving more observation to the significant parts of the signal. We first present the definition of edge expander codes or graphs.

As shown in Fig. 2, an (α and δ) unbalanced bipartite edge expander graph is a bipartite graph (G, A, and B) with n left variable nodes, m right check nodes, and minimal and maximal left degrees $d_{\min}$ and $d_{\max}$, respectively, such that for any subset $X \subset A$ with $|X| \le \alpha n$ has at least $N(X) = \delta|\Gamma(X)|$ neighbors, where $\Gamma(X)$ is the set of edges that connect X and $N(X)$, and δ is the expansion factor[21]. Especially, if the left nodes hold the same degree, the above definition has the same formulation with Ref. [21], which is considered as an uniform sampling scheme. Normally, the relationship between the variable nodes and check nodes are represented by the adjacency matrix $\Phi \in \mathrm{R}^{m\times n}$, that is, if the check node i connects to variable node j, $\Phi_{ij} = 1$, otherwise, $\Phi_{ij} = 0$. Actually, a randomly chosen bipartite graph will probably be a good edge expander[22].

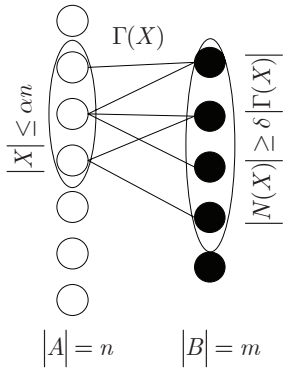

Fig. 2. Illustration of an (α and δ) edge expander code, A and B correspond to the set of signal elements and the set of measurements, respectively. The measuring process can be modeled as the adjacency matrix.

The unbalanced expander graphs can well simulate the processing of sparse sampling, the left vertices correspond to the elements of the original signal, and the right vertices are equivalent to the compressive measurements. Moreover, the adjacency matrices of the expander graphs are considered as the measurement matrices instead of the conventional dense random matrices. Jafarpour *et al.*[21] proposed that the adjacency matrices of the (α and δ) expanders with same left degrees are efficient measurement matrices due to the satisfaction of l_1-norm restricted isometry property. As mentioned above, we want the significant parts of the sparse signals to be taken more measurement times, that is, the corresponding left vertices will have more neighbors in the right part of the edge expanders. Assuming we roughly know the positional information of the significant elements of a given sparse signal, the following conclusion holds for edge expander graphs framework.

Let $\Phi \in \mathrm{R}^{m\times n}$ be the adjacency matrix of an (α and δ) edge expander, S is a subset of left vertices set, each vertex in S has $d_{\max}$ right neighbors, and the rest have $d_{\min}$ each. Given an αn sparse signal $x \in \mathrm{R}^n$ (which has only αn nonzero elements), if the left vertices corresponding to the nonzero elements of the signal are all included in S, then

$$(2\delta - 1)\|x\|_1 \le \left\|\left(\Phi / d_{\max}\right)x\right\|_1 \le \|x\|_1 . \tag{1}$$

The proof of the above conclusion is nearly the same as that of Theorem 1 in Ref. [21]. The above conclusion not only implies the adjacency matrices of edge expanders can be used as measurement matrices for sparse sampling framework but also reveals the expansion factor δ is the most important parameter for such expanders. To verify the performance of different edge expanders with different left degrees, we need to calculate the expansion factors first. Consider a given subset of left vertices $X' \subset A$, the corresponding neighbors set is $N(X') = \left\{r_j \in B \middle| v_i \in X' \text{and} \, e_{ij} \in \Gamma(X')\right\}$. In terms of the adjacency matrix Φ, $\Phi_{X'}$ is the submatrix of

Φ composed of columns of Φ indexed by the set X', so the number of neighbors of X' is the number of rows in $\Phi_{X'}$ with at least one nonzero, denoted by $\left|\Phi^1_{X'}\right|$, and the number of edges that X' connects is the number of value 1 in $\Phi_{X'}$, denoted by $\left|\Phi_{X'}\right|$. Then we can define the expansion of an edge expander as the ratio $\left|N(X')\right|/\left|\Gamma(X')\right|$, or $\left|\Phi^1_{X'}\right|/\left|\Phi_{X'}\right|$. Notice that $\left|\Phi^1_{X'}\right|$ and $\left|\Phi_{X'}\right|$ are random variables depending on X', thus we can acquire a statistical result of expansion by randomly selecting X' many times.

As an example, a 256 × 256 tissue phantom image is designed and shown in Fig. 3(a), if we regard every column of the image as a signal, the crucial coefficients are always in the middle position. If the important coefficients are scattered, the support set can be estimated as the union of some focused index sets. We let the support set of every column be $S = [50, 160]$ in this case, corresponding to an expander graph with 256 left vertices, the vertices in the support set will have more neighbors. Figure 3(b) shows a schematic of 100 0-1 masks designed by such edge expander with $d_{\max} = 30$, $d_{\min} = 8$, and $m = 100$. Each optic mask is obtained by extending each row of the matrix to a 256 × 256 matrix. Based on the support set, there are more value 1 in the corresponding index set of the mask, which means more optic energy is absorbed by the corresponding tissue. In addition, we use $\left|\Phi^1_{X_1}\right|/\left|\Phi^1_{X_2}\right|$ to measure the expansion of different expanders with different degrees, where $X_1 \subset S$ and $X_2 \subset A\backslash S$ and are with the same size. Figure 3(c) shows plots of the mean values of $\left|\Phi^1_{X_1}\right|/\left|\Phi^1_{X_2}\right|$ for different sizes of $\left|X_1\right|$ (or $\left|X_2\right|$) and different degrees taken over 500 realizations. As can be seen, for the uniform sampling case ($d_{\max} = d_{\min}$), the measurements for zero elements and nonzero elements are nearly the same. For non-uniform sampling case ($d_{\max} > d_{\min}$), the measurements for nonzero elements are dramatically more than that of zero elements, and when increasing $d_{\max}$, the gap will also increase. Moreover, essentially beyond a certain bound, there is no gain in increasing $d_{\max}$ because $d_{\max}$ will be very close to m.

In CSPAT, we measure integrals over patterns or collections of points. The measurements V_k at the kth arc position after m expander masks can be expressed as a linear equation $V_k = \widehat{\Phi} U_k + N_k$, where matrix $\widehat{\Phi} \in R^{m\times n}$ denotes the linear forward operator related

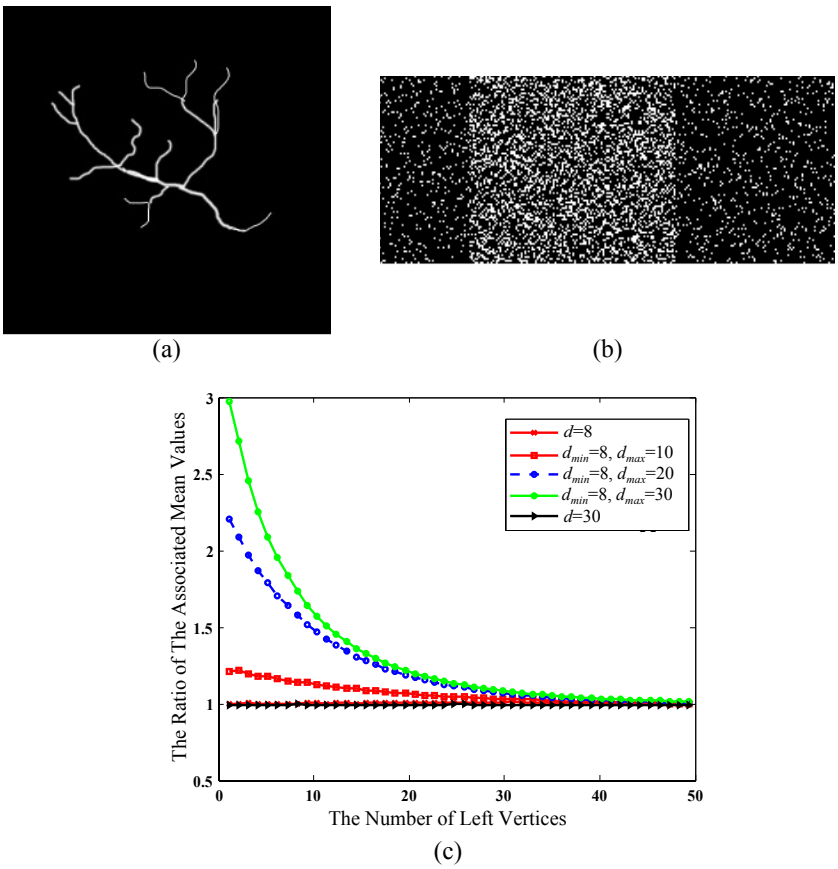

Fig. 3. (a) 2D tissue phantom image, (b) 100 masks designed from the adjacent matrix of an edge expander, each row of the 0-1 matrix can extend to be a 256 × 256 matrix as a mask, and (c) comparison of the mean values of $\left|\Phi^1_{X_1}\right|/\left|\Phi^1_{X_2}\right|$ for different sizes of $\left|X_1\right|$ (or $\left|X_2\right|$), and different degrees taken over 500 realizations. The curves imply the nonzero element sets with the same sizes are observed more times in non-uniform sampling case.

to the optic mask Φ[10,15], U_k is the corresponding PA signal to be reconstructed and N_k is the measurement noise often modeled as white Gaussian noise. We can also model the problem as $V=\widehat{\Phi}U+N$, where $U \in R^{n\times n}$ is considered as the desired image, the kth column of V and N are V_k and N_k, respectively. To solve this ill-conditioned model fitting problem (because of insufficient measurements), some non-quadratic regularization (or widely known as sparsity constraints) should be used to incorporate prior information into the reconstruction process. In this work, we consider the widely used total variation (TV) as the regularization term. TV has been demonstrated effective in improving reconstruction quality because of the advantages in terms of edge preservation and noise removal[23]. Based on TV regularization, we propose to estimate U using

$$\hat{U} = \arg\min_{U} \left\| V - \hat{\Phi} U \right\|_2^2 + \lambda \left\| \nabla U \right\|_1 , \tag{2}$$

where $\lambda > 0$ is a regularization parameter, $\left\|\nabla U\right\|_1$ is the TV regularization term defined as $\left\|\nabla U\right\|_1 = \Sigma_{ij} \left|(\nabla U)_{ij}\right| = \Sigma_{ij} \sqrt{\left|(\nabla^1 U)_{ij}\right|^2 + \left|(\nabla^2 U)_{ij}\right|^2}$, ∇^1 and ∇^2 denote horizontal and vertical difference operators[23], respectively. Several algorithms can solve the optimization problem expressed as Eq. (2), we propose to use an efficient primal-dual-based algorithm described in Ref. [23].

The aforementioned tissue phantom has been used to evaluate the performance of the proposed framework (please refer Refs. [14,15] for further details on the phantom). We used k-wave toolbox to model PA propagation in tissue, and all reconstructions were implemented in MATLAB. The simulative mask changes its optical absorption distribution pattern based on the well-designed edge expander codes for each laser light pulse. And it can be realized as the time-varying switch array and modulated according to the 0–1 adjacent matrices of expander codes (or other random 0–1 matrices) by the computer in real application. To better evaluate the performance, the relative l_2 reconstruction error defined as $E_r = \left\|U - U_0\right\|_2 / \left\|U_0\right\|_2$ was used to compare different reconstructions, where $\widehat{U}$ is the reconstructed image and U_0 denotes the reference image. Figures 4(a)–(d) show a set of representative simulation results obtained by different methods with 60 masks and signal-to-noise ratios (SNRs) of 10 dB. The method non-uniform (8, 30) is corresponding to the edge expander mask mentioned earlier with $d_{\min} = 8$, $d_{\max} = 30$, and for uniform case, $d_{\min} = d_{\max}$. As can be seen, non-uniform sampling reconstruction demonstrates better visual quality than uniform sampling and random sampling reconstructions. Furthermore, the l_2 reconstruction errors for random, uniform (8, 8), uniform (30, 30), and non-uniform (8, 30) are 0.7198, 0.7211, 0.7080, and 0.6532, respectively, which can further demonstrate the improvement of the proposed method.

A more comprehensive comparison of the relative l_2 reconstruction errors for different mask patterns with different number of measurements (noisy observation with SNR = 10 dB) is shown in Fig. 4(e). Since all four kinds of masks were randomly chosen, the experimental results for each number of measurement were averaged 50 times. The curves further show that the proposed method uses fewer measurements to achieve the same error than other methods tested. To further validate the proposed method, we compared it with two other methods in Ref. [14], that is, Bayesian compressive sensing (BCS) algorithm and basis pursuit (BP) with random masks. Table 1 shows the reconstruction performances of the three methods with SNR = 10 dB in terms of reconstruction error and running time. As can be seen, with the same number of masks, the proposed method

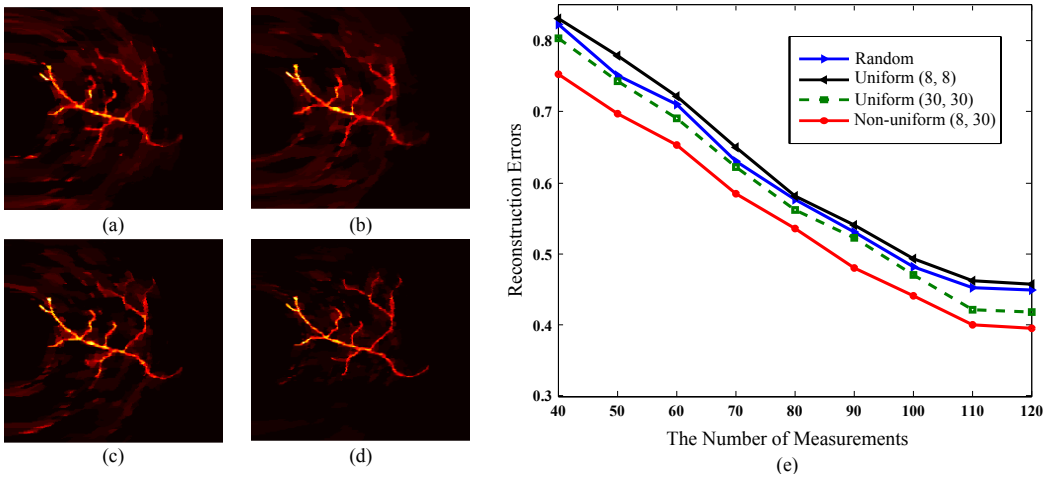

Fig. 4. Simulation results from (a) 60 random masks, (b) uniform (8, 8) expander masks, (c) uniform (30, 30) expander masks, and (d) non-uniform (8, 30) expander masks, respectively and (e) relative l_2 errors for different methods at different number of measurements.

Table 1. Reconstruction Performances of Different Methods with SNR = 10 dB in Terms of Reconstruction Error E_r and Computing Time t

Methods	**BP + Random Masks**		**BCS + Random Masks**		**Proposed**	
Number of Masks	E_r	t (s)	E_r	t (s)	E_r	t (s)
40	0.8764	22.1522	0.8072	14.8883	0.7523	5.1455
60	0.7324	23.8244	0.6889	15.5615	0.6246	5.2511
80	0.6457	24.5351	0.5788	16.0241	0.5354	5.7037

has better reconstruction quality and significantly fewer computing times than the other two methods.

In conclusion, we present an edge expander codes-based method to design the optic masks for CSPAT, and propose a TV regularization-based model to formulate the associated problem. The proposed method aims to reduce the number of measurements and reconstruct the images from limited view acquisition by giving more observation to the significant parts. A similar idea using limited view PA data for reconstruction is applied to reconstruct the images of the subcutaneous vasculature of human hand, the subcutaneous vasculature of the back of a rat. Both theoretical analysis and results from carefully designed computer simulations demonstrate the effectiveness of the proposed method, so we expect the proposed method to put into practice and to provide an approach for optimal mask design and be an integral part of CSPAT. For further study, we will consider the case that the support set spans a very large area, that is, the image is not sparse at all.

This work was supported by the National Natural Science Foundation of China (Nos. 61174016, 61201307, and 61371045) and the Fundamental Research Funds for the Central Universities (No. HIT. NSRIF. 2013132).

References

1. X. D. Wang, Y. J. Pang, G. Ku, X. Y. Xie, G. Stoica, and L. V. Wang, Nat. Biotechnol. **21,** 803 (2003).
2. H. F. Zhang, K. Maslov, G. Stoica, and L. V. Wang, Nat. Biotechnol. **24,** 848 (2006).
3. J. M. Yang, C. Favazza, R. M. Chen, J. J. Yao, X. Cai, K. Maslov, Q. F. Zhou, K. K. Shung, and L. V. Wang, Nat. Med. **18,** 1297 (2012).
4. L. V. Wang and S. Hu, Science **335,** 1458 (2012).
5. C. G. Lou, S. H. Yang, Z. Ji, Q. Chen, and D. Xing, Phys. Rev. Lett. **109,** 218101 (2012).
6. F. Gao, Y. J. Zheng, X. H. Feng, and C. D. Ohi, Appl. Phys. Lett. **102,** 063702 (2013).
7. S. Kellnberger, M. Omar, G. Sergiadis, and V. Ntziachristos, **103,** 153706 (2013).
8. X. H. Feng, F. Gao, and Y. J. Zheng, **103,** 083704 (2013).
9. J. Provost and F. Lesage, IEEE Trans. Med. Imaging **28,** 585 (2009).
10. D. Liang, H. F. Zhang, and L. Ying, Int. J. Function. Inform. Personal. Med. **2,** 394 (2009).
11. J. Meng, L. V. Wang, D. Liang, and L. Song, Opt. Lett. **37,** 4573 (2012).
12. J. Meng, L. V. Wang, L. Ying, D. Liang, and L. Song, Opt. Express **20,** 16510 (2012).
13. J. Meng, C. B. Liu, J. X. Zheng, R. Q. Lin, and L. Song, J. Biomed. Opt. **19,** 036003 (2014).
14. M. Sun, N. Feng, Y. Shen, J. Li, L. Ma, and Z. Wu, Chin. Opt. Lett. **9,** 1 (2011).
15. M. J. Sun, N. Z. Feng, Y. Shen, X. L. Shen, L. Y. Ma, J. G. Li, and Z. H. Wu, Opt. Express **19,** 14801 (2011) .
16. N. Huynh, E. Zhang, M. Betcke, S. Arridge, P. Beard, and B. Cox, in *Proceedings of Photons Plus Ultrasound: Imaging and Sensing* (2014).
17. D. L. Donoho, IEEE Trans. Inf. Theory **52,** 1289 (2006).
18. M. F. Duarte and Y. C. Eldar, IEEE Trans. Signal Process. **59,** 4053 (2011).
19. Y. Liu, X. Q. Zhu, L. Zhang, and S. H. Cho, Sensors **12,** 13034 (2012).
20. M. Wang, W. Y. Xu, and A. Tang, IEEE Trans. Signal Process. **59,** 1007 (2012).
21. S. Jafarpour, W. Y. Xu, B. Hassibi, and R. Calderbank, IEEE Trans. Inf. Theory **55,** 4299 (2009).
22. M. Sipser and D. A. Spielman, IEEE Trans. Inf. Theory **42,** 1710 (1996).
23. A. Chambolle and T. Pock, J. Math. Imaging Vision **40,** 120 (2011).